Influences of Random Surface Waves on the Estimates of Wind Energy Input to the Ekman Layer in the Antarctic Circumpolar Current Region

Yuming Zhang[1,2] [iD], **Zhaoyang Song[3]** [iD], **Kejian Wu[4]**, and **Yongfang Shi[5,6]**

[1]National Marine Environmental Monitoring Center, Ministry of Ecology and Environment of the People's Republic of China, Dalian, China, [2]Key Laboratory of Global Change and Marine-Atmospheric Chemistry, State Oceanic Administration, Xiamen, China, [3]GEOMAR Helmholtz Centre for Ocean Research Kiel, Kiel, Germany, [4]College of Oceanic and Atmospheric Sciences, Ocean University of China, Qingdao, China, [5]The First Institute of Oceanography, Ministry of Natural Resources, Qingdao, China, [6]National Laboratory for Marine Science and Technology, Qingdao, China

Abstract Sea surface waves significantly affect the wind energy input to the Ekman layer in the upper ocean. In the study, we first incorporated the wave-induced Coriolis-Stokes forcing, the reduction of wind stress caused by wave generation, and wave dissipation into the classical Ekman model to investigate the kinetic energy balance in the wave-affected Ekman layer. Then, both the theoretical steady state solution for the idealized condition and the nonsteady state solution for the realistic ocean were derived. Total energy input to the wave-affected Ekman layer includes the wind stress energy input and the wave-induced energy input. Based on the WAVEWATCH III model, the wave spectrum was simulated to represent realistic random directional wave conditions. The wind stress energy input and the wave-induced energy input to the wave-affected Ekman layer in the Antarctic Circumpolar Current in the period from 1988 to 2010 were then calculated. The annual mean total energy input in the Antarctic Circumpolar Current region was 402.5 GW and the proportions of the wind stress energy input and the wave-induced energy input were, respectively, 85% and 15%. Particularly, total energy input in the Antarctic Circumpolar Current in the wave-affected Ekman layer model was 59.8% lower than that in the classical Ekman model. We conclude that surface waves play a significant role in the wind energy input to the Ekman layer.

Plain Language Summary The wind energy input to the Ekman layer is one major source to balance the dissipation of mechanical energy in the ocean. Sea surface waves significantly influence the wind energy input to the Ekman layer. Previous studies only considered the Stokes drift induced by surface waves based on a simple monochromatic assumption. This study derived a realistic nonsteady state solution by incorporating three surface wave-related processes: wave-induced Coriolis-Stokes forcing, the reduction of wind stress caused by wave generation, and wave dissipation into the classical Ekman model. A numerical model was employed to simulate the wave spectra representing the realistic random surface waves. The total energy input in the Antarctic Circumpolar Current region from 1988 to 2010 was estimated. The estimated total energy input was 59.8% lower than that in the classical Ekman model, indicating that surface waves significantly affected the wind energy input in the Ekman layer.

1. Introduction

Estimates of the wind energy input to the surface geostrophic current (Wunsch, 1998), near-inertial motions (Alford, 2003; Rimac et al., 2013, 2016; Watanabe & Hibiya, 2002), and subinertial motions (Wang & Huang, 2004) indicate the importance of wind stress in driving a variety of physical processes in the ocean surface layer. In the upper ocean, the Ekman layer is forced directly by surface winds. Thus, the dissipation of mechanical energy in the Ekman layer is mainly balanced by the wind energy input. Wang and Huang (2004) investigated the wind energy input to the classical Ekman layer (hereafter defined as WH04 model) and estimated global distribution of the wind energy input. However, this model did not include the influence of surface waves. In addition, observations revealed different vertical structures of Ekman spiral from the classical Ekman theory (Lewis & Belcher, 2004; Polton et al., 2005; Price & Sundermeyer, 1999). Moreover, surface waves largely determine the observed Ekman current profiles via the Stokes drift and mixing (Lewis & Belcher, 2004; Polton et al., 2005; Rascle et al., 2006). Therefore, the influences of surface

waves should be considered in the estimation of the wind energy input to the subinertial motions in the Ekman layer.

Liu et al. (2007) incorporated the Coriolis-Stokes forcing into WH04 model to obtain the Stokes-Ekman layer model and assessed global wind energy input to subinertial motions with this improved model. The assessment results showed that surface waves contributed 12% of the total energy input. Wu and Liu (2008) further investigated the wind energy input in the Antarctic Circumpolar Current (ACC) region and reported that the Stokes drift-induced energy input accounted for approximately 22% of the total energy input. Based on the report by Liu et al. (2007), Polton (2009) modified the wave averaging process in the energy budget for the Stokes-Ekman layer model. Liu et al. (2009) revised the energy budget following Polton (2009) and derived the corrected Stokes-Ekman layer model (hereafter defined as the Liu09 model). Based on Liu09 model, some researchers further explored the wind energy input to the ACC region and western Mediterranean Sea and found that the Coriolis-Stokes forcing could substantially alter the relative contributions of wave-induced Stokes drift and surface wind to the energy balance of Ekman layer (Sayol et al., 2016; Zhang et al., 2013).

However, these aforementioned studies had the same deficiency. A monochromatic wave condition was assumed in these studies, so the Stokes drift was based on an empirical estimate. Tamura et al. (2012) found that such assumption resulted in the underestimation of surface Stokes drift (50%–90% smaller) and the overestimation of the Stokes depth (5–20 times larger), which led to an inaccurate estimate of wave-induced energy input. In addition, Song (2009) suggested that the Stokes drift, wave dissipation, and the reduced wind stress caused by the generated surface waves affected the Ekman current as well as the estimation of wind energy input. The Stokes drift affects both the depth and the mean flow in the mixed layer (Lewis & Belcher, 2004). It deforms the vortices associated with the mixed layer turbulence, thus enhancing turbulent kinetic energy and regulating the depth of the mixed layer. Additionally, it deforms the planetary vorticity in the horizontal momentum equations, thus altering the mean flow in the mixed layer (Lewis & Belcher, 2004). Except the Stokes drift, surface waves also influence the ocean current via other processes. The temporal and spatial variabilities of surface waves reveal the structure and variations of the driving wind stress fields, and interact with ocean currents. When waves break and dissipate, momentum transfers from waves to ocean currents (Song, 2009).

To achieve more accurate estimates of wind energy input, we deduced an improved expression for the wind energy input in the wave-affected Ekman layer. First, three wave-induced terms (the Stokes drift, the reduction of wind stress caused by wave generation, and wave dissipation) were incorporated for the subsequent estimation. Then, the state-of-the-art wave model, WAVEWATCH III, was employed to simulate wave spectra. Hence, three wave-induced terms for the random directional waves could be directly calculated under realistic wave conditions (Ardhuin et al., 2009; Kantha et al., 2009; Rascle et al., 2008; Tamura et al., 2012; Webb & Fox-Kemper, 2011), thus improving the estimations of wind stress energy and wave-induced energy inputs by reducing the errors caused by inaccurate Stokes drift estimation.

Both WH04 and Liu09 models gave the steady state energy input solutions for the idealized steady wind conditions and the nonsteady state solutions for the time-dependent wind forcing conditions. Similarly, we also derived these two solutions. The steady state solution exhibits the way that each individual wave-induced term affects the wind energy input, whereas the nonsteady state solution is used to estimate the wind energy input to the realistic ocean. Our study focused on the ACC region. As reported by Wang and Huang (2004), the ACC region received the largest wind energy input. This region is particularly sensitive to anthropogenic climate change, as evidenced by significantly strengthened westerly wind stress (Lin et al., 2018). The Southern Ocean is characterized by swell-dominated seas with high significant wave heights driven by frequent storms (Lund et al., 2017; Young, 1999). Both processes contribute to the energy exchange in the upper ocean and atmosphere. However, the wind stress energy input and wave-induced energy input as well as its variability over the ACC region were understudied.

This paper is organized as follows. Section 2 deduces the steady and nonsteady state solutions of wind stress energy and wave-induced energy inputs in the Ekman layer. Section 3 illustrates the estimation of the total energy input into the Ekman layer within the ACC region based on the hindcast experiment of wave model. Section 4 gives the brief summary and discussion.

2. Methods and Experimental Setup

2.1. Energy Balance in the Wave-Affected Ekman Layer

For the incompressible Eulerian flow $\mathbf{v}$, the governing equation of horizontal momentum is expressed as

$$\rho\frac{\partial \mathbf{v}}{\partial t} + \rho\mathbf{v}\cdot\nabla\mathbf{v} + \rho\mathbf{f}\times\mathbf{v} = -\nabla p + \rho\mathbf{X}, \tag{1}$$

where $\mathbf{f}$ is the Coriolis parameter; p is the pressure; ρ is the water density; t is the time; and $\mathbf{X}$ refers to the divergence of the Reynolds stresses, that is, $X_i = \partial\{v_i' v_j'\}/\partial x_j$. Here $\mathbf{v}$ can be decomposed into two parts: a steady horizontally homogeneous part $\mathbf{U}$ and a wave component $\widetilde{\mathbf{u}}$.

According to Ardhuin et al. (2008), $\mathbf{X}$ is expressed as

$$X_i = \frac{\partial}{\partial z}\left(A_z\frac{\partial U_i}{\partial z}\right) - T_i^{ds}. \tag{2}$$

where z is the depth, A_z denotes the vertical eddy viscosity, and T^{ds} represents wave-induced momentum transferred from waves to ocean currents due to the dissipation of wave energy (Jenkins, 1987, 1989).

The scalar product of equation (1) with $\mathbf{v}$ is obtained and then applied in the wave averaging, as suggested by Polton (2009). The energy equation of the Ekman layer is deduced as

$$\rho\frac{\partial}{\partial t}\frac{\mathbf{U}^2}{2} + \rho\frac{\partial}{\partial z}(\mathbf{f}\times\mathbf{T}_S\cdot\mathbf{U}) = \rho A_z\mathbf{U}\cdot\frac{\partial^2\mathbf{U}}{\partial z^2} - \rho\mathbf{U}\cdot\mathbf{T}^{ds}, \tag{3}$$

$$\mathbf{T}_S(z) = \int_{-\infty}^{z}\mathbf{U}_S(z)dz, \tag{4}$$

where $\mathbf{T}_S(z)$ is the Stokes transport, $\mathbf{U}_S = (U_{Sx}, U_{Sy})$ is the Stokes drift vector (refer to the Appendix), and $\mathbf{T}^{ds} = \left(T_x^{ds}, T_y^{ds}\right)$ is the wave dissipation vector. The second term in the left of equation (3) represents the effect of Coriolis-Stokes forcing.

Then, the boundary conditions in the wave-affected Ekman equation by Tang et al. (2007) are applied in equation (3),

$$A_z\frac{\partial \mathbf{U}}{\partial z}\bigg|_{z=0} = \frac{\boldsymbol{\tau}_a}{\rho} - \frac{\boldsymbol{\tau}_{in}}{\rho}, \tag{5}$$

$$\mathbf{U}|_{z\to-\infty} = 0, \tag{6}$$

where $\boldsymbol{\tau}_a = (\tau_{ax}, \tau_{ay}) = \rho_a C_d|U_{10}|\mathbf{U}_{10}$ is the wind stress, computed from 10-m wind speed $\mathbf{U}_{10}$, density ρ_a, and air-sea drag coefficient $C_d = (0.8 + 0.065U_{10})\times 10^{-3}$ (Wu, 1982); $\boldsymbol{\tau}_{in} = (\tau_{inx}, \tau_{iny})$ is the reduction of wind stress caused by wave generation. $\boldsymbol{\tau}_{in}$ is converted as (Jenkins, 1989; Tang et al., 2007)

$$\boldsymbol{\tau}_{in} = \rho\int\left(\frac{\omega}{k}\right)\mathbf{k}S_{in}(k,\theta)dkd\,\theta, \tag{7}$$

where ω is the wave frequency; k and $\mathbf{k}$ are, respectively, the wave number and wave number vector; θ is the wave direction; and $S_{in}(k,\theta)$ represents the source term of the wind input to the surface waves and is defined as (Hasselmann et al., 1988)

$$S_{in}(k,\theta) = C_{in}\frac{\rho_a}{\rho}\max\left[0,\left(\frac{28u_*}{c}\cos(\theta-\theta_W)-1\right)\right]\omega E(\mathbf{k},\theta), \tag{8}$$

$$u_* = |U_{10}|\sqrt{C_d}, \tag{9}$$

where C_{in} is a constant and equals 0.25, θ_W is the mean wind direction, u_* is the wind friction velocity, and $E(k,\theta)$ is the wave spectrum and discussed later. According to Donelan et al. (2012), the frictional drag and

the wave drag are the two types of momentum transfer between atmosphere and ocean. Parameter τ_{in} indicates the wave drag due to the wave generation. The wave drag arises from waves and becomes larger as the wave steepness increases. The steeper the waves are, the larger the contribution of the wave drag to the total drag is.

Integrating equation (3) from the bottom to the surface, the energy balance of the wave-affected Ekman layer is expressed as

$$\frac{\partial E}{\partial t} = E_w + E_S - D, \tag{10}$$

where

$$E = \int_{-\infty}^{0} \frac{\rho}{2} \mathbf{U}^2 dz, \tag{11}$$

$$E_w = (\boldsymbol{\tau}_a - \boldsymbol{\tau}_{in}) \cdot \mathbf{U}(0), \tag{12}$$

$$E_S = -\rho \mathbf{f} \times \mathbf{T}_S(0) \cdot \mathbf{U}(0), \tag{13}$$

$$D = \int_{-\infty}^{0} \rho A_z \left| \frac{\partial \mathbf{U}}{\partial z} \right|^2 dz + \int_{-\infty}^{0} \rho \mathbf{U} \cdot \mathbf{T}^{ds} dz. \tag{14}$$

Equations (12)–(15) denote the total kinetic energy in the wave-affected Ekman layer, the wind stress energy input, the wave-induced energy input, and the energy dissipation process, respectively. $\mathbf{U}(0)$ represents the horizontal velocity at the sea surface in the wave-affected Ekman layer.

2.2. Steady State Solution

For the random directional waves, the parameterizations for the Stokes drift and wave dissipation are provided in the Appendix in order to simplify the deduction process of the analytical solutions of the wind stress energy and wave-induced energy inputs. The steady state solutions reveal the way that surface waves influence the energy balance of the Ekman layer through different processes.

Song (2009) presented the analytic steady solutions of the wave-affected Ekman equations, in which the eddy viscosity coefficient was set to be either depth-independent or proportional to depth. In this study, the parameterization for the depth-independent eddy viscosity coefficient was adopted. This parameterization scheme was initially proposed by Ekman (1905) and further verified by 16-month field observations in the Pacific (Santiago-Mandujano & Firing, 1990):

$$A_z = 1.2 \times 10^{-4} U_{10}^2. \tag{15}$$

Song (2009) gave the complex wave-affected Ekman solution at the sea surface as follows:

$$U(0) = \frac{\tau_a - \tau_{in}}{j\rho A_z} \frac{1}{jA_z} \int_{-\infty}^{0} \left\{ if\, U_S(z') + T^{ds}(z') \right\} \cosh(jz') dz'$$
$$+ \frac{1}{jA_z} \int_{-\infty}^{0} \left\{ if\, U_S(z') + T^{ds}(z') \right\} \sinh(-jz') dz', \tag{16}$$

where

$$j = \begin{cases} \dfrac{1}{d_e}(1+i), f > 0 \\ \dfrac{1}{d_e}(1-i), f < 0 \end{cases}, \tag{17}$$

$d_e = \sqrt{\frac{2A_z}{|f|}}$ is the depth of the Ekman layer; f is the scalar of the Coriolis parameter; and $\tau_a = \tau_{ax} + i\tau_{ay}$, $\tau_{in} = \tau_{inx} + i\tau_{iny}$, $U_S = U_{Sx} + iU_{Sy}$, and $T^{ds} = T_x^{ds} + iT_y^{ds}$ are the complex variables. Combining the

parameterizations for the Stokes drift $\mathbf{U}_S^p(z) = \mathbf{U}_{S0} \exp\left(\frac{z}{d_S}\right)$ and the wave dissipation $\mathbf{T}^{ds,p}(z) = \mathbf{T}_0^{ds} \exp\left(\frac{z}{d_{ds}}\right)$ shown in the Appendix, equation (17) is converted as

$$U(0) = \frac{\tau_a - \tau_{in}}{j\rho A_z} - \frac{ifU_{S0}}{jA_z(1/d_S + j)} - \frac{T_0^{ds}}{jA_z(1/d_{ds} + j)}, \tag{18}$$

where U_{S0} is the complex Stokes drift velocity at the sea surface; T_0^{ds} is the complex wave dissipation at the sea surface; d_S is the Stokes e-folding depth, and it is used to represent the penetration depth of Stokes drift for random directional wavefield and defined as

$$U_S(z=-d_S) \Big/ U_{S0} = \exp(-1), \tag{19}$$

d_{ds} is the e-folding depth of wave dissipation and defined as

$$T^{ds}(z=-d_{ds}) \Big/ T_0^{ds} = \exp(-1). \tag{20}$$

Based on the aforementioned wave-affected Ekman solution (equation (19)), the wind stress energy input in the wave-affected Ekman layer (equations (S1)–(S14) in the supporting information) is expressed as

$$E_w = E_{w1} + E_{w2} + E_{w3}, \tag{21}$$

where

$$E_{w1} = \frac{|\tau_a - \tau_{in}|^2}{\rho d_e |\mathbf{f}|}, \tag{22}$$

$$E_{w2} = \frac{1}{cs^2 + 2cs + 2} \cdot \{-(cs+2)(\tau_a - \tau_{in}) \cdot \mathbf{U}_{S0} + \mathrm{sgn}(f) \cdot cs \cdot \widehat{\mathbf{z}} \cdot [(\tau_a - \tau_{in}) \times \mathbf{U}_{S0}]\}, \tag{23}$$

$$E_{w3} = -\frac{1}{|f|(cds^2 + 2cds + 2)} \cdot \{cds(\tau_a - \tau_{in}) \cdot \mathbf{T}_0^{ds} + \mathrm{sgn}(f) \cdot (cds+2) \cdot \widehat{\mathbf{z}} \cdot [(\tau_a - \tau_{in}) \times \mathbf{T}_0^{ds}]\} \tag{24}$$

Note that $\widehat{\mathbf{z}}$ is the upward unit vector; $\mathbf{U}_{S0}$ and $\mathbf{T}_0^{ds}$ represent the vectors of U_{S0} and T_0^{ds}, respectively; and sgn $(f) = \begin{cases} 1, f>0 \\ -1, f<0 \end{cases}$. These vectors are defined as

$$\mathbf{U}_{S0} = 2\int \mathbf{k} E(k,\theta) dk d\theta, \tag{25}$$

$$\mathbf{T}_0^{ds} = 2\int \omega \mathbf{k} S_{ds}(k,\theta) dk d\theta. \tag{26}$$

where $S_{ds}(k,\theta)$ is the dissipation source term and denotes the wave energy dissipation that is converted to the currents within the water column (Hasselmann et al., 1988 and Komen et al., 1995),

$$S_{ds}(k,\theta) = -2.25\omega(k^2 m_0)^2 \left[\frac{k}{k} + \left(\frac{k}{k}\right)^2\right] E(k,\theta), \tag{27}$$

where

$$m_0 = \iint E(k,\theta) dk d\theta, \tag{28}$$

$$\langle\omega\rangle = \left[m_0^{-1} \iint E(k,\theta)\omega^{-1} dk d\theta\right]^{-1}, \tag{29}$$

$$\langle k\rangle = \left[m_0^{-1} \iint E(k,\theta)k^{-1} dk d\theta\right]^{-2}. \tag{30}$$

Here we define two nondimensional variables $cs = d_e \big/ d_S$ and $cds = d_e \big/ d_{ds}$. Hence, the wind stress energy input in the wave-affected Ekman layer E_w is composed of the following three terms: E_{w1} (the wind

energy input in the wave-affected Ekman layer due to wind stress), E_{w2} (the interaction between the wind stress and the Stokes drift), and E_{w3} (the interaction between the wind stress and the wave dissipation, which refers to the influence of the momentum transferred from waves to the mean flow on the wind energy input). The three wave-induced terms, $\mathbf{U}_S$, τ_{in}, and $\mathbf{T}^{ds}$, influence different processes of the wind stress energy input. In particular, τ_{in} linearly weakens the wind stress and affects all three terms of the wind stress energy input, whereas $\mathbf{U}_S$ and $\mathbf{T}^{ds}$ affect the wind stress energy input through their interactions with the wind stress.

The wave-induced energy input E_S can be decomposed into three components (equations (S15)–(S27)):

$$E_S = E_{S1} + E_{S2} + E_{S3}, \tag{31}$$

where

$$E_{S1} = \frac{d_S \cdot \rho |f| \cdot cs |\mathbf{U}_{S0}|^2}{cs^2 + 2cs + 2}, \tag{32}$$

$$E_{S2} = \frac{1}{cs} \{ \text{sgn}(f) \cdot \widehat{\mathbf{z}} \cdot [(\tau_a - \tau_{in}) \times \mathbf{U}_{S0}] + (\tau_a - \tau_{in}) \cdot \mathbf{U}_{S0} \}, \tag{33}$$

$$E_{S3} = \frac{d_S \cdot \rho}{cds^2 + 2cds + 2} \{ \text{sgn}(f) \cdot cds \cdot \widehat{\mathbf{z}} \cdot (\mathbf{U}_{S0} \times \mathbf{T}_0^{ds}) - (cds + 2)\mathbf{U}_{S0} \cdot \mathbf{T}_0^{ds} \}. \tag{34}$$

E_{S1} is mainly related to the velocity of the Stokes drift, the depth of the Ekman layer, and the Stokes e-folding depth; E_{S2}, which is comparable to E_{w2}, denotes the interaction between the wind stress and the Stokes drift; and E_{S3} represents the interaction between the Stokes drift and the wave dissipation.

Thus, the total energy input to the wave-affected Ekman layer E_t is

$$E_t = E_w + E_S. \tag{35}$$

2.2.1. Influence of Surface Waves

Next, we discuss the individual influences of three wave-induced terms on the steady state solution of the total energy input to the wave-affected Ekman layer. First, we assume a minor influence of the wave dissipation term $\mathbf{T}^{ds}$. Then, E_{w3} and E_{S3} can be neglected. Thus, the wind stress energy input is given as

$$E'_w = E_{w1} + E_{w2}, \tag{36}$$

and the Stokes drift-induced energy input is expressed as

$$E'_S = E_{S1} + E_{S2}. \tag{37}$$

If the term τ_{in} is neglected, the wind stress energy input to the Ekman layer is the same as that in the Liu09 model:
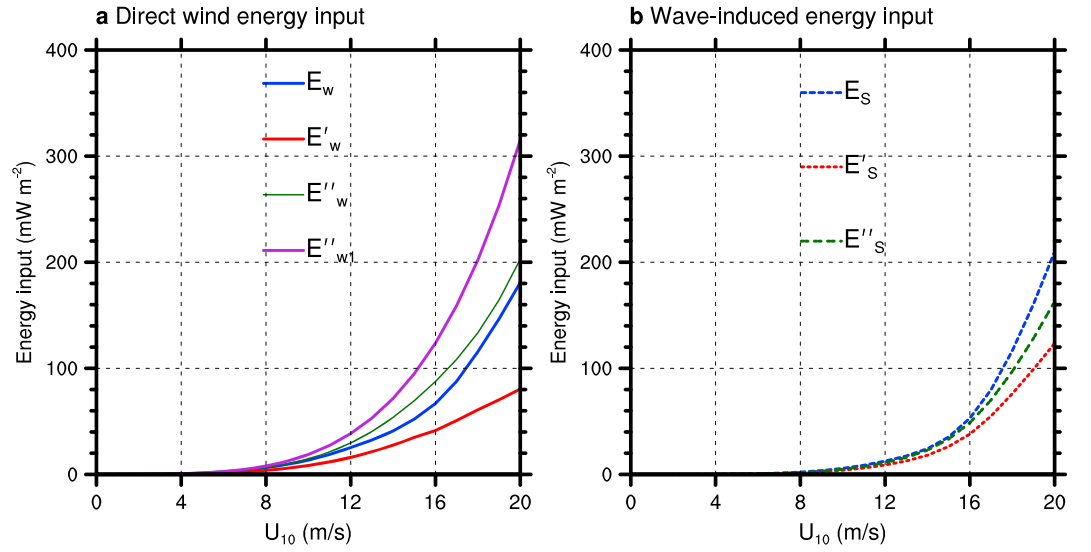
$$E''_w = E''_{w1} + E''_{w2}, \tag{38}$$

where

$$E''_{w1} = \frac{|\tau_a|^2}{\rho d_e |f|}, \tag{39}$$

$$E''_{w2} = \frac{1}{cs^2 + 2cs + 2} \cdot [-(cs + 2)\tau_a \cdot \mathbf{U}_{S0} + \text{sgn}(f) \cdot cs \cdot \widehat{\mathbf{z}} \cdot (\tau_a \times \mathbf{U}_{S0})], \tag{40}$$

where E''_{w1} denotes the classical wind energy input to the Ekman layer without considering the influence of surface waves (Wang & Huang, 2004). The wave-induced energy input in the Ekman layer is deduced according to the Liu09 model,

Figure 1. (a) Wind stress energy inputs and (b) wave-induced energy inputs to the Ekman layer as a function of 10-m wind speed U_{10} at latitude 45°. In Figure 1a, E_w and E'_w represent the wind stress energy inputs to the wave-affected Ekman layer with and without considering the influence of wave dissipation. E''_w and E''_{w1} refer to the wind stress energy inputs in the Liu09 model and WH04 model. In Figure 1b, E_S and E'_s indicate the wave-induced energy inputs in the wave-affected Ekman layer model with and without incorporating the wave dissipation term, respectively. E''_s indicates the wave-induced energy input in the Liu09 model. The unit is mW/m^2 (1 mW/m$^2 = 10^{-3}$ W/m^2).

$$E''_S = E_{S1} + E''_{S2}, \tag{41}$$

where

$$E''_{S2} = \frac{1}{cs} \left[\text{sgn}(f) \cdot \hat{\mathbf{z}} \cdot (\boldsymbol{\tau}_a \times \mathbf{U}_{S0}) + \boldsymbol{\tau}_a \cdot \mathbf{U}_{S0} \right]. \tag{42}$$

Then, we calculate the total energy input in the wave-affected Ekman layer based on a fully developed wind-generated surface wave described by the wave number spectrum (Donelan & Pierson, 1987):

$$E(k,\theta) = \frac{0.00162 \times U_{10}}{k^{2.5} g^{0.5}} \exp\left[-\frac{g^2}{k^2 (1.2U_{10})^4} \right] 1.7^{\Gamma} \times h\left(\frac{k}{k_p}\right) \text{sech}^2\left[h\left(\frac{k}{k_p}\right)(\theta - \theta_w) \right],$$
$$(0 < k < 10k_p, \quad -\pi < \theta < \pi), \tag{43}$$

where θ_w is the wind direction.

$$\Gamma = \exp\left[-1.22 \left(\frac{1.2U_{10} k^{0.5}}{g^{0.5}} - 1 \right)^2 \right], \tag{44}$$

$$h = \begin{cases} 1.24, & 0 < k/k_p < 0.31 \\ 2.61 \left(k/k_p \right)^{0.65}, & 0.31 < k/k_p < 0.90 \\ 2.28 \left(k_p/k \right)^{0.65}, & 0.90 < k/k_p < 10 \end{cases}. \tag{45}$$

The wave number of the peak in the spectrum is

$$k_p = g \Big/ (1.2U_{10})^2, \tag{46}$$

where U_{10} is the scalar of 10-m wind speed.

Figure 1 illustrates the wind stress energy (Figure 1a) and wave-induced energy inputs (Figure 1b) in the Ekman layer as a function of wind speed at the latitude of 45°, which is the latitude of ACC. The E_w in

Figure 1a represents the estimate of wind stress energy input to the wave-affected Ekman layer deduced in this study. E'_w indicates the wind stress energy input to the wave-affected Ekman layer without considering the influence of wave dissipation. E''_w and E''_{w1} refer to the wind stress energy inputs in the Liu09 model and the WH04 model, respectively. The wind stress energy input in these Ekman layer models all increase rapidly with the increase in wind speed (Figure 1a). As illustrated in the wave-affected Ekman layer model in this study, when the wind speed increases from 10 to 15 m/s, the wind stress energy input (E_w) increases from 13.5 mW/m^2 (1 mW/m^2 = 10^{-3} W/m^2) to 52.1 mW/m^2. The wind stress energy input in the wave-affected Ekman layer model (E_w) is much weaker than the wind energy input in the classical WH04 model (E''_{w1}), especially under high wind speed conditions (Figure 1a). E'_w illustrates the much weaker energy input and suggests the importance of the interaction between the wind stress and the wave dissipation in enhancing wind energy input in the wave-affected Ekman layer. According to Tang et al. (2007), when waves dissipate, although the mechanical energy may be dissipated as heat, the horizontal components of the momentum are conserved under dissipative processes. The momentum can be transferred to the mean flow, which is represented as T^{ds}. Thus, wave dissipation enhances the wind energy input in the wave-affected Ekman layer. The reduction of wind stress caused by wave generation (τ_{in}) weakens the wind energy input, thus leading to the difference between the curves of E'_w and E''_w in the Liu09 model.

The wave-induced energy input can be quantified in the Liu09 model and the wave-affected Ekman layer model (Figure 1b). The wave-induced energy input in the wave-affected Ekman layer model (E_S) increases rapidly from 5.7 to 35.3 mW/m^2 when the wind speed increases from 10 to 15 m/s. The difference between E'_s (without considering the influence of wave dissipation) and E''_s (the wave-induced energy input in the Liu09 model) indicates that the reduction in wind stress caused by wave generation (τ_{in}) weakens the wave-induced energy input. Compared with E''_s, E_S becomes much larger because the wave dissipation term (T^{ds}) strongly enhances the wave-induced energy input. The difference between E'_s and E_S is larger than the difference between E'_s and E''_s, indicating that the enhancing effect of wave dissipation on wave-induced energy input is more significant than the reduction effect of wind stress on wave-induced energy input (Figure 1b).

To further investigate the relative importance of the wave-induced energy (E_S) to the wind stress energy (E_w) input in the wave-affected Ekman layer model, a parameter is defined as $R = \frac{E_s}{E_w}$. Figure 2 illustrates the variation of this ratio with the 10-m wind speed at different latitudes.

The parameter R increases rapidly along with the increase in wind speed and latitude (Figure 2), indicating that the wave-induced energy is rather large at high latitudes and/or under high wind speed conditions. The theoretical solution shows that the wave-induced energy input is larger than the wind stress energy input ($R > 1$ in Figure 2) at the latitude of 60° when the wind speed reaches 16 m/s. This implies that wave-induced energy input is crucial in the ACC region. Additionally, in the wave-affected Ekman layer model (Figure 2a), R is 0.1–0.5 larger than that in the Liu09 model (Figure 2b), suggesting that τ_{in} and T^{ds} are of significant importance to the wave-induced energy input. Thus, these terms should be considered in the evaluation of the influence of waves on the wind energy input to the Ekman layer. The result highlights the importance of surface waves. However, this solution is only applicable to the steady state, a highly idealized condition in which wind speed or wind direction does not vary with time. Therefore, this solution cannot be applied in the realistic ocean.

2.3. Nonsteady State Solution

As the wind forcing at the ocean surface is time-varying, the motions in the Ekman layer are in nonsteady states. Therefore, the steady state solution is not realistic. To provide the better approximation for related variables in the nonsteady state solution, we adopted the Fourier series expansions as $\mathbf{U} = \sum_{|\omega_n|<\omega_c} \mathbf{U}_n \exp(i\omega_n t)$, $\mathbf{U}_s = \sum_{|\omega_n|<\omega_c} \mathbf{U}_{S,n} \exp(i\omega_n t)$, $\tau_a = \sum_{|\omega_n|<\omega_c} \tau_{a,n} \exp(i\omega_n t)$, $\tau_{in} = \sum_{|\omega_n|<\omega_c} \tau_{in,n} \exp(i\omega_n t)$, and $\mathbf{T}^{ds} = \sum_{|\omega_n|<\omega_c} \mathbf{T}^{ds}_n \exp(i\omega_n t)$, where ω_n is the frequency with $\omega_c = 0.5$ cycle/day the cutoff frequency. The cutoff frequency is the same as that in WH04 and Liu09 models, which take the steady state and subinertial motions into account (Wang & Huang, 2004). Note that $\omega_n < 0$ ($\omega_n > 0$) indicates clockwise (anticlockwise) rotating wind. $\omega_n = 0$ represents the steady component.
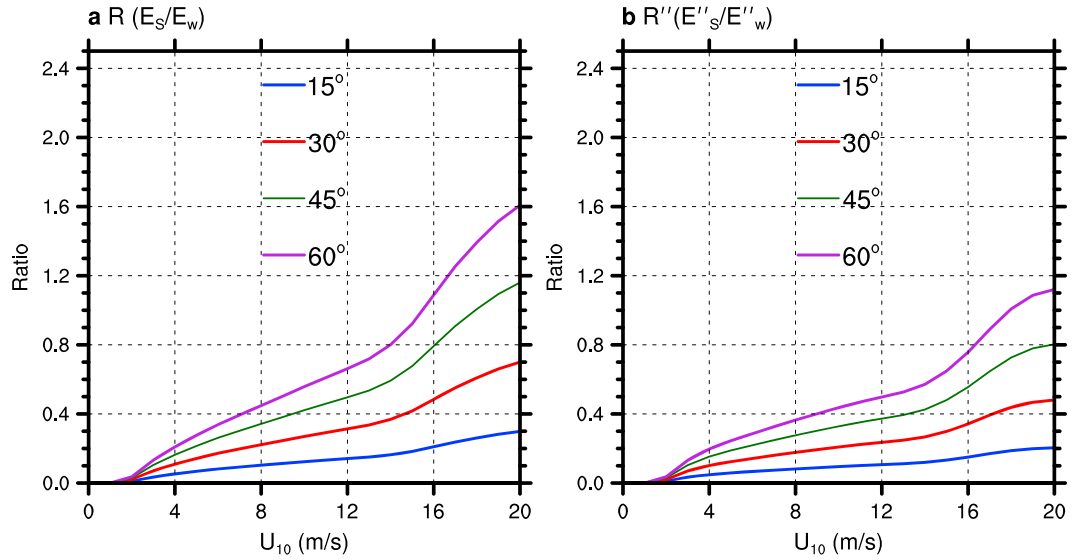
Figure 2. Ratio of the wave-induced energy input to the wind stress energy input as a function of 10-m wind speed U_{10} for the latitudes 15°, 30°, 45°, and 60° in (a) the wave-affected Ekman layer and (b) the Liu09 model, respectively.

The nonsteady state solution of the wind stress energy input in the wave-affected Ekman layer model is expressed as

$$E_w = \sum_n E_w^n = \sum_n \left(E_{w1}^n + E_{w2}^n + E_{w3}^n\right), \tag{47}$$

where

$$E_{w1}^n = \frac{|\boldsymbol{\tau}_{a,n} - \boldsymbol{\tau}_{in,n}|^2}{\rho d_e^n |f + \omega_n|}, \tag{48}$$

$$E_{w2}^n = \frac{f}{\left(cs_n^2 + 2cs_n + 2\right)(f + \omega_n)} \cdot \left\{-(cs_n + 2)\left(\boldsymbol{\tau}_{a,n} - \boldsymbol{\tau}_{in,n}\right) \cdot \mathbf{U}_{S0,n} + \operatorname{sgn}(f + \omega_n) \cdot cs_n \cdot \widehat{\mathbf{z}} \cdot \left[\left(\boldsymbol{\tau}_{a,n} - \boldsymbol{\tau}_{in,n}\right) \times \mathbf{U}_{S0,n}\right]\right\}, \tag{49}$$

$$E_{w3}^n = -\frac{1}{|f + \omega_n|\left(cds_n^2 + 2cds_n + 2\right)} \cdot \left\{cds_n\left(\boldsymbol{\tau}_{a,n} - \boldsymbol{\tau}_{in,n}\right) \cdot \mathbf{T}_{0,n}^{ds} + \operatorname{sgn}(f + \omega_n) \cdot (cds_n + 2) \cdot \widehat{\mathbf{z}} \cdot \left[\left(\boldsymbol{\tau}_{a,n} - \boldsymbol{\tau}_{in,n}\right) \times \mathbf{T}_{0,n}^{ds}\right]\right\}. \tag{50}$$

The wave-induced energy input to the wave-affected Ekman layer is expressed as

$$E_S = \sum_n E_S^n = \sum_n \left(E_{S1}^n + E_{S2}^n + E_{S3}^n\right), \tag{51}$$

where

$$E_{S1}^n = \frac{d_{S,n} \cdot \rho \cdot cs_n |\mathbf{U}_{S0,n}|^2}{cs_n^2 + 2cs_n + 2} \cdot \frac{f^2}{|f + \omega_n|}, \tag{52}$$

$$E_{S2}^n = \frac{f}{cs_n(f + \omega_n)} \left\{\operatorname{sgn}(f + \omega_n) \cdot \widehat{\mathbf{z}} \cdot \left[\left(\boldsymbol{\tau}_{a,n} - \boldsymbol{\tau}_{in,n}\right) \times \mathbf{U}_{S0,n}\right] + \left(\boldsymbol{\tau}_{a,n} - \boldsymbol{\tau}_{in,n}\right) \cdot \mathbf{U}_{S0,n}\right\}, \tag{53}$$

$$E_{S3}^n = \frac{d_{S,n} \rho f}{\left(cds_n^2 + 2cds_n + 2\right)(f + \omega_n)} \left\{\operatorname{sgn}(f + \omega_n) \cdot cds_n \cdot \widehat{\mathbf{z}} \cdot \left(\mathbf{U}_{S0,n} \times \mathbf{T}_{0,n}^{ds}\right) - (cds_n + 2) \mathbf{U}_{S0,n} \cdot \mathbf{T}_{0,n}^{ds}\right\}. \tag{54}$$

Here the parameters of the nth component are defined as $d_{e,n} = \sqrt{\frac{2A_z}{|f + \omega_n|}}$, $d_S = \sum_{|\omega_n| < \omega_c} d_{S,n} \exp(i\omega_n t)$, $d_{ds} = \sum_{|\omega_n| < \omega_c} d_{ds,n} \exp(i\omega_n t)$, and $cs_n = \frac{d_{e,n}}{d_{S,n}}$, $cds_n = \frac{d_{e,n}}{d_{ds,n}}$.

2.4. Hindcast Experiment

With the WAVEWATCH III (WW3) model (version 3.14), a hindcast experiment was conducted to provide wave spectra for the estimation of wave-induced terms and the associated wind energy input in the Ekman layer. The horizontal resolution is on a 1°×1° rectilinear grid, ranging from 78°N to 78°S without the poles. We adopted the source terms by Tolman and Chalikov (1996) and the discrete interaction approximation method by Hasselmann et al. (1985) in the hindcast experiment. These schemes were the same as those by Tamura et al. (2012). The wave spectrum was equally discretized from 0° to 360° in 36 directions ($\Delta\theta = 10°$). The spectrum consists of 35 frequencies ranging from 0.041 to 1.05 Hz with a logarithmic increment by $f_{n+1} = 1.1f_n$, where f_n is the nth frequency.

The hindcast experiment was integrated for 23 years from 1988 to 2010 with the Cross-Calibrated Multi-Platform (CCMP) ocean surface wind data set (Atlas et al., 2009). The initialization time in the model is one month (from 1 December of the previous year). The ocean bathymetry and shape of coastlines are from the ETOPO1 data set. The wave spectrum in the Southern Ocean (from 30°S to 78°S) is 6-hourly output at a resolution of 2°×2°.

According to the report by Tamura et al. (2012), we examined the simulation results of the surface Stokes drift in our hindcast experiment. Given that there were no available wave spectral observations in the ACC region, we adopted six buoys from the National Data Buoy Center (https://www.ndbc.noaa.gov/historical_data.shtml) deployed in the deep northern Pacific for validation (Table S1). The root-mean-square error (defined as the difference between the estimated surface Stokes drift based on simulated wave spectra and that based on the observed wave spectra) was less than 4.5 cm/s (Table S2). The correlation coefficients of the simulated and observed surface Stokes drift ranged from 0.74 to 0.94 at all locations (Table S2). These metrics suggested that the hindcast experiment was sufficiently robust to represent the wave density spectra and surface Stokes drift field.

3. Results

Figure 3 shows the annual mean wind stress (Figure 3a) and the simulated annual mean surface Stokes drift in the Southern Ocean (Figure 3b). The velocity of the Stokes drift is largely attributed to the wind stress. Both wind stress and surface Stokes drift are quite strong in the southern Indian Ocean (40–60°S, 30–120°E). With regard to the direction, the mean Stokes drift is toward the east. The direction is consistent with the westerly wind in the midlatitudes. We then calculated the wave-induced variables, such as the reduction of wind stress caused by wave generation (τ_{in}), the surface Stokes drift ($\mathbf{U}_{S0}$) and its e-folding depth (d_S), and wave dissipation ($\mathbf{T}_0^{ds}$) and its e-folding depth (d_{ds}), from the wave spectrum data based on equations (8), (26), (27), (20), and (21). With these estimates of wave-induced variables, the total energy input to the wave-affected Ekman layer was assessed with equations (48)–54.

3.1. Contributions of Wave-Induced Terms

We investigated the contributions of wave-induced terms to the wind stress energy (Figure 4) and wave-induced energy inputs (Figure 5) in the wave-affected Ekman layer from 1988 to 2010.

E_{w1} represents the contribution of direct wind stress to the wind stress energy input and is the main part of E_w, equals an area-weighted average of 4.77 mW/m² in the ACC region (Figure 4a). Here we confined the ACC region from 40°S to 60°S. E_{w2} has an average negative contribution of −0.42 mW/m² (Figure 4b). E_{w2} indicates the interaction between the wind stress and the surface Stokes drift, so this negative value suggests that the interaction reduces the wind stress energy input. Meanwhile, this interaction increases the wave-induced energy input (E_{S2}) by 0.39 mW/m² (Figure 5b). The interaction between the wave dissipation and the wind stress (E_{w3}) positively contributes 1.65 mW/m² to the wind stress energy input (Figure 4c), whereas the interaction between the wave dissipation and the Stokes drift (E_{S3}) positively contributes 0.51 mW/m² to the wave-induced energy inputs (Figure 5c). In relative to the Stokes drift (Figure 5a) and the reduced wind stress (Figure 5b), the wave dissipation is one major wave-induced process which is responsible for the wave-induced energy input in the wave-affected Ekman layer (Figure 5c).
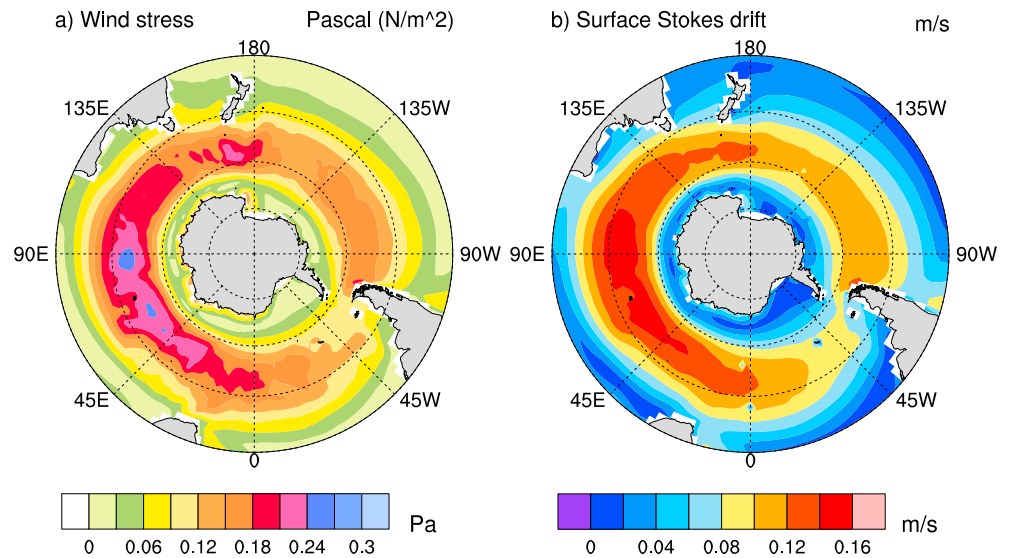
Figure 3. Distributions of the 23-year averaged (a) wind stress τ_a (unit: Pa) and (b) surface Stokes drift U_{S0} (unit: m/s) in the Southern Ocean.
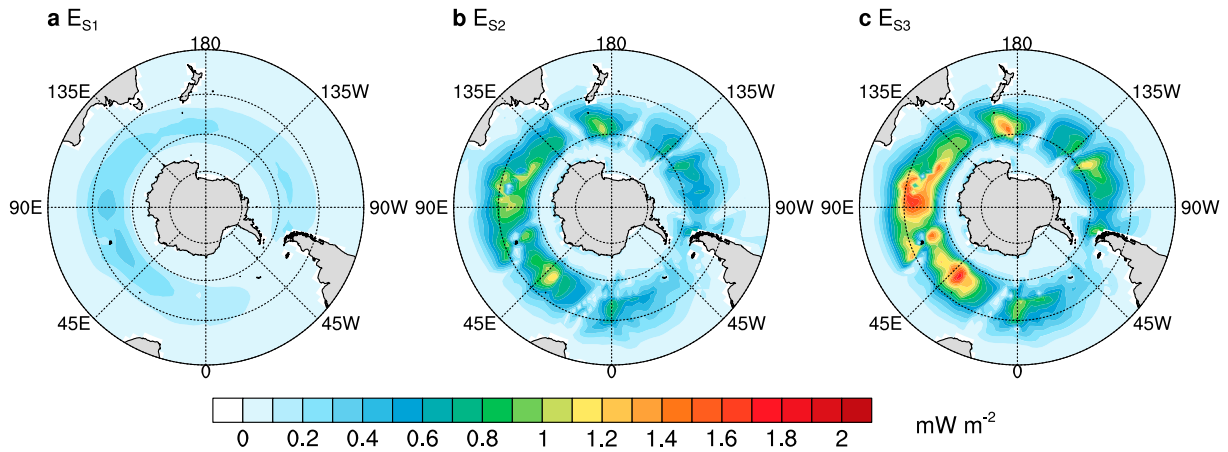
3.2. Wind Energy Inputs in the Classical and Wave-Affected Ekman Layer

We compared the total energy input in the wave-affected Ekman layer model with that in the classical WH04 model to investigate the influences of surface waves.

Figure 6 illustrates the annual mean energy inputs estimated both in the WH04 model (Figure 6a) and the wave-affected Ekman layer model (Figures 6b–6d) from 1988 to 2010. The WH04 model shows intensive wind energy input (E_{w1}'') in the southern Indian Ocean (40–60°S, 30–120°E) and the southwest Pacific Ocean (40–60°S, 150°E–80°W). The wind energy input in the South Atlantic (40–60°S, 60°W–30°E) was relatively modest (Figure 6a). The spatial distributions of the wind stress energy input (Figure 6b), wave-induced energy input (Figure 6c), and total energy input (Figure 6d) in the wave-affected Ekman layer model were similar to the wind energy input in the WH04 model (Figure 6a). In the wave-affected Ekman layer, compared to the wave-induced energy input (Figure 6c), the wind stress energy input (Figure 6b) was still the dominant energy source. The total energy input in the wave-affected Ekman layer (Figure 6d) was much weaker than that in the classical WH04 model (Figure 6a), suggesting that the wind energy input was greatly reduced due to the generation of surface waves (Figure 1). We then calculated the total energy input to the
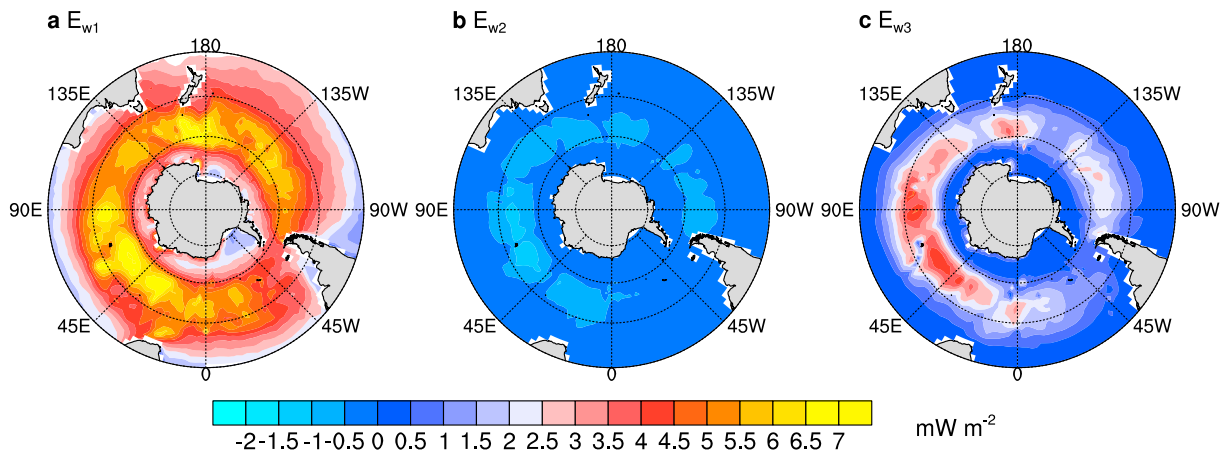
Figure 4. Annual mean contributions of (a) the direct wind stress (E_{w1}), (b) the interaction of the wind stress with the Stokes drift (E_{w2}), and (c) the interaction of the wind stress with the wave dissipation (E_{w3}) to the wind stress energy input (unit: mW/m^2) in the wave-affected Ekman layer from 1988 to 2010.

Figure 5. Annual mean contributions of (a) the Stokes drift (E_{S1}), (b) the interaction of the Stokes drift with the wind stress (E_{S2}), and (c) the interaction of the Stokes drift with the wave dissipation (E_{S3}) to the wave-induced energy input (unit: mW/m^2) in the wave-affected Ekman layer from 1988 to 2010.
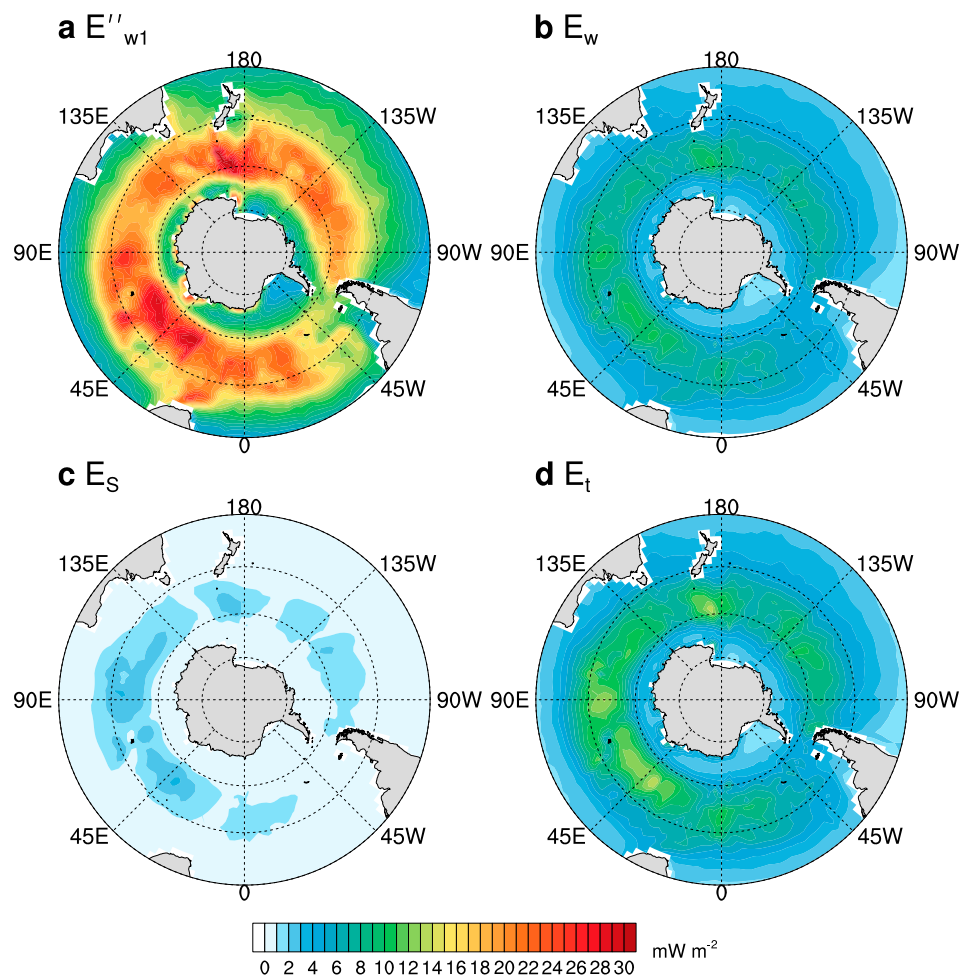
Figure 6. Annual mean wind energy input (unit: mW/m^2) in the Ekman layer in the Southern Ocean from 1988 to 2010. (a) Wind energy input in the classical WH04 model (E''_{w1}), (b) the wind stress energy input (E_w), (c) wave-induced energy input (E_S), and (d) total energy input (E_t) in the wave-affected Ekman layer model. The wind stress energy input (E_w) is the sum of E_{w1} (Figure 4a), E_{w2} (Figure 4b), and E_{w3} (Figure 4c). The wave induced energy input (E_S) is the sum of E_{S1} (Figure 5a), E_{S2} (Figure 5b), and E_{S3} (Figure 5c).

Table 1
Overview of Total Energy Input, the Wind Stress Energy Input, and Wave-Induced Energy Input in the Antarctic Circumpolar Current (40–60°S) Region Estimated by Four Models

	Wind Stress Energy Input	Wave-Induced Energy Input	Total Energy Input
WH04	1000.5 (E_{w1}'')		1000.5
Liu09	956.4 (E_w'')	47.9 (E_S'')	1004.3 (E_t'')
Wave-affected Ekman layer^{OD}	247.0 (E_w')	29.9 (E_S')	276.9 (E_t')
Wave-affected Ekman layer	342.8 (E_w)	59.7 (E_S)	402.5 (E_t)

Note that the wave-affected Ekman layer^{OD} refers to the wave-affected Ekman layer without considering the impact of wave dissipation. The unit is GW.

Liu09 model based on the CCMP wind data set (Table 1). The 23-year averaged total energy input in the ACC region was 1004.3 GW, consisting of the wind stress energy input (956.4 GW) and wave-induced energy input (47.9 GW). Compared to the wave-affected Ekman layer, Liu09 model overestimated the wind stress energy input by 613.6 GW and underestimated the wave-induced energy input by 11.8 GW. To further quantify the contribution of wave dissipation process, the estimates of total energy input in the wave-affected Ekman layer without considering wave dissipation was calculated (Table 1). Both the wind stress energy and wave-induced energy inputs were reduced by 95.8 GW (28%) and 29.8 GW (50%), compared to those in the wave-affected Ekman layer. The data suggested the significant influences of wave generation and wave dissipation processes on the wind energy input in the upper ocean.

With regard to the meridional distributions of total energy inputs, both the WH04 model and the wave-affected Ekman layer model illustrated the maxima at 52°S. The result was consistent with the spatial distribution of surface wind stress and the surface Stokes drift (Figure 3). In terms of the zonal distribution, the total energy input reached its maximum in the southern Indian Ocean and its minimum near the Drake Passage at approximately 63°W, thus demonstrating the influence of land-sea distribution on the westerly wind and surface wave development (Figures 3 and 6).

3.3. Variability of the Wind Energy Input in the Wave-Affected Ekman Layer
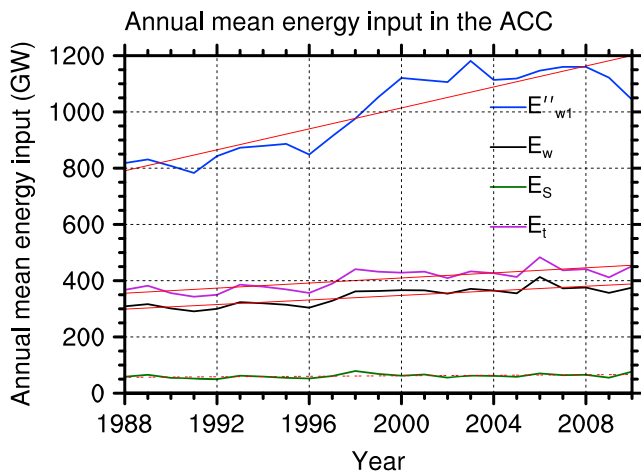
Figure 7. Time series of area-weighted annual mean wind energy input (unit: GW, 1 GW = 10^9 W) in the ACC region in the WH04 and the wave-affected Ekman layer model. E_{w1}' represents the wind energy input in the classical WH04 model. E_w, E_S, and E_t represent the wind stress energy input, wave-induced energy input, and total energy input in the wave-affected Ekman layer model, respectively. The red lines indicate the trend (unit: GW/year) of wind energy input calculated from the linear regression from 1988 to 2010. The solid trend indicates that the trend is significant at the 95% confidence level in Student's t test and vice versa for the dashed trend.

In this section, we discussed the variability of the total energy input in the Ekman layer. Figure 7 shows the time series of annual area-weighted sum of total energy inputs from 1988 to 2010 in the ACC region. The wind energy input (E_{w1}'') in the WH04 model varied greatly from year to year. The standard deviation of the annual mean wind energy input in the ACC region in the WH04 model was up to 140.7 GW. In contrast, the wind stress energy input (E_w), wave-induced energy input (E_S), and the total energy input (E_t) in the wave-affected Ekman layer demonstrated higher stability (Figure 7). Their standard deviations were only 32.4, 7.5, and 37.9 GW, respectively. The generation of surface waves and their interaction with surface wind substantially stabilized the wind energy inputs in the upper ocean. The annual mean wind energy input (E_{w1}'') in the ACC region in the WH04 model significantly increased at a rate of 18.6 GW/year from 1988 to 2010 (Figure 7). The increasing rate was significant at the 95% confidence level according to the result of Student's t test. The 23-year annual mean wind stress energy input (E_w) in the wave-affected Ekman layer was 402.5 GW, illustrating a modestly increasing trend of 4.1 GW/year from 1988 to 2010 (Figure 7). In general, the wave-induced energy input (E_S) in the wave-affected Ekman layer was quite stable in the same period, displaying insignificant changes (Figure 7). The total energy input (E_t) was increased at a rate of 4.5 GW/year due to the main contribution of the wind stress energy input.

Table 2 summarizes seasonal mean wind energy inputs in the southern Indian, Pacific and Atlantic Oceans, and the ACC region. The wind

Table 2
Overview of the Seasonal Mean Wind Energy Input in Different Basins

SON	JJA	MAM	DJF		
293.4 ± 43.3	369.8 ± 51.8	271.7 ± 36.5	183.6 ± 21.8	E''_{w1}	Southern Indian
110.1 ± 11.9	136.1 ± 15.9	101.4 ± 11.0	71 ± 6.6	E_w	
27.1 ± 4.0	35.2 ± 7.3	23.7 ± 4.6	14.9 ± 2.2	E_S	
137.2 ± 15.3	171.3 ± 22.0	125.0 ± 14.9	85.9 ± 8.4	E_t	
327.9 ± 52.7	396.0 ± 65.6	357.0 ± 55.6	233.7 ± 24.2	E''_{w1}	Southern Pacific
118.6 ± 17.4	129.4 ± 22.6	125.2 ± 18.4	86.3 ± 7.8	E_w	
24.0 ± 7.4	19.7 ± 9.5	23.0 ± 6.0	15.5 ± 3.1	E_S	
142.6 ± 24.1	149.1 ± 31.4	148.2 ± 24.0	101.8 ± 10.5	E_t	
233.4 ± 35.6	335.4 ± 55.0	242.9 ± 46.6	160.9 ± 17.2	E''_{w1}	Southern Atlantic
80.6 ± 8.3	108.6 ± 10.8	82.4 ± 10.6	58.8 ± 4.5	E_w	
12.6 ± 2.4	17.2 ± 2.7	12.8 ± 2.1	9.1 ± 1.5	E_S	
93.3 ± 10.1	125.7 ± 12.4	95.2 ± 12.3	67.9 ± 5.7	E_t	
961.6 ± 133.7	1223.8 ± 172.0	981.5 ± 143.6	655.2 ± 63.4	E''_{w1}	ACC
347.9 ± 34.3	416.2 ± 42.1	349.4 ± 39.1	244.7 ± 16.5	E_w	
71.9 ± 11.4	80.2 ± 16.3	68.0 ± 10.4	44.8 ± 5.1	E_S	
419.9 ± 43.2	496.4 ± 54.5	417.4 ± 47.8	289.5 ± 20.3	E_t	

The area-weighted December-January-February (DJF), March-April-May (MAM), June-July-August (JJA), and September-October-November (SON) mean wind energy input (unit: GW) and the uncertainties in the southern Indian Ocean (40–60°S, 30°E–120°E), southern Pacific Ocean (40–60°S, 150°E–80°W), southern Atlantic Ocean (40–60°S, 60°W–30°E), and ACC (40–60°S, 180°W–180°E) region are listed. E''_{w1} represents the wind energy input in the WH04 model. E_w, E_S, and E_t indicate the wind stress energy input, wave-induced energy input, and total energy input in the wave-affected Ekman layer model, respectively.

energy inputs in both the WH04 model and wave-induced Ekman layer model showed pronounced seasonal variations (Table 2). In austral summer, the wind energy input in the WH04 model reached its minimum throughout the year. The area-weighted sum of the wind energy input (E''_{w1}) in the ACC region was only 655.2 GW (Table 2). With regard to the spatial variation, the sum of area-weighted wind energy input in the southern Indian (40–60°S, 30–120°E), southern Pacific (40–60°S, 150°E–80°W), and southern Atlantic (40–60°S, 60°W–30°E) were 183.6, 233.7, and 160.9 GW, respectively. Similarly, the total energy input in the wave-affected Ekman layer model was the least in the austral summer and included the wind stress energy input (244.7 GW) and wave-induced energy input (44.8 GW). The southern Pacific and southern Indian Ocean received seasonal total energy inputs of 101.8 and 85.9 GW, respectively. The total energy input in the southern Atlantic (67.9 GW) was the least among three basins. The seasonal total energy input and its spatial variations are the strongest in the austral winter. With regard to the classical WH04 model, the June-July-August mean wind energy input in the ACC area was 1,223.8 GW. Particularly, the area-weighted wind energy inputs in the southern Indian, Pacific, and Atlantic Oceans were 369.8, 396.0, and 335.4 GW, respectively. Compared to the WH04 model, the wave-affected Ekman layer model gave the much lower total energy input in the ACC region including the wind stress energy (416.2 GW) and the wave-induced energy input (80.2 GW). The contributions of the total energy inputs into the southern Indian, Pacific, and Atlantic Oceans were 171.3, 149.1, and 125.7 GW, respectively. In the wave-induced Ekman layer model, the wave-induced energy input contributed 17% of the variational amplitude of the total energy input (Table 2).

4. Summary and Discussion

We investigated the influences of ocean surface waves on the wind energy input in the Ekman layer and estimated the wind energy input in the ACC region with the nonsteady state solution derived from a wave-affected Ekman layer model. This model was obtained by incorporating three processes associated with surface waves into the classical Ekman layer model. These processes consist of the generation of surface Stokes drift caused by surface wind stress, the interaction between the wind stress and surface waves, and the interaction of wind stress with the wave dissipation. In the estimation of the Stokes drift, we adopted the simulated spectrum with the WAVEWATCH III model based on random directional waves and driven by the CCMP winds other than the monochromatic wave assumption, thus avoiding the

underestimation of surface Stokes drift and the overestimation of the Stokes depth (Tamura et al., 2012). Therefore, the wind energy input based on the wave-affected Ekman layer model from 1988 to 2010 was estimated. The 23-year annual mean area-weighted total energy input in the ACC region was 402.5 GW, including 342.8 GW for wind stress energy and 59.7 GW for wave-induced energy input. In this period, the total energy input in the ACC region illustrated a significantly increasing trend, which was consistent with the strengthening wind stress. The total energy input also demonstrated a pronounced annual variation, with its maximum in austral winter and minimum in austral summer. The seasonal maximum total energy input was 1.7 times of the minima.

With the wave-affected Ekman model, we investigated the influences of surface waves on the wind energy input to the Ekman layer. The wind energy input was divided into two parts: the wind stress energy input and wave-induced energy input. The wave-induced energy input was an important energy source, especially in the ACC region, and contributed approximately 15% of the total energy input. Moreover, the estimated total energy input in the wave-affected Ekman layer model was 59.8% weaker than that obtained in the classical Ekman model (WH04 model) and 59.9% weaker than that obtained in the Liu09 model. The difference between the wave-affected Ekman layer model and the WH04 model was mainly ascribed to the weakening of wind stress via the wave generation, whereas the difference between the wave-affected Ekman layer model and the Liu09 model highlighted the influences of wind-wave interaction and wave dissipation on the wind energy input in the upper ocean.

Consistent with Huang et al. (2006), our results revealed the increasing total energy input in the ACC from 1988 to 2010. The increase could be attributed to the enhancing wind stress over the Southern Ocean (Figure S1). The annual mean zonal wind stress from CCMP data averaged between 40°S and 60°S increased by 10% from 1988 to 2010. Consistently, Yang et al. (2008) found that the zonal wind stress between 45°S and 65°S was significantly intensified from 1980 to 1999 in both the National Centers for Environmental Prediction–National Center for Atmospheric Research reanalysis and the 40-year European Centre for Medium-Range Weather Forecasts reanalysis data. Such strengthening westerly winds over the Southern Ocean could be associated with global warming (Swart et al., 2015; Swart & Fyfe, 2012). Additionally, the spatial distributions of the total energy input in the ACC reached its maximum in the southern Pacific Ocean and minimum in the southern Atlantic Ocean and were consistent with the spatial characteristic of the CCMP wind stress data set and surface Stokes drift from the hindcast experiment. The narrow Drake Passage constrained the development of surface waves and resulted in the less wind energy input in the southern Atlantic Basin.

Finally, this study was based on the assumption that the eddy viscosity was independent of depth. The relation had been extensively applied in the studies on the upper ocean, including high sea-state and high wind conditions (Hui & Xu, 2016; Perrie et al., 2003). However, Elipot and Gille (2009) pointed out that this highly idealized relationship seemed inappropriate in real ocean applications due to the overestimation of viscosity. As indicated by Song (2009), the vertical structure of eddy viscosity could significantly modify the angular turning of the Ekman surface current. Therefore, in the future, we will develop a scheme with varying eddy viscosity as a function of the water depth in order to improve the estimates of the mechanical wind energy input in the upper ocean.

Appendix A: Parameterizations for the Stokes Drift and the Wave Dissipation

To simply the calculation of the Stokes drift and the wave dissipation, we parameterize two variables.

Under deepwater conditions, assuming a statistically stationary and horizontally homogeneous wavefield, the bulk formulation of the Stokes drift profile for a monochromatic wave with the frequency ω, wave number k, and wave amplitude A is (Philips, 1977)

$$\mathbf{U}_S^b(z) = \mathbf{U}_{S0}^b \exp\left(\frac{z}{d_S^b}\right), \quad \mathbf{U}_{S0}^b = \omega \mathbf{k} A^2, \tag{A.1}$$

where $\mathbf{U}_{S0}^b$ is the Stokes drift at the sea surface in the bulk formulation and $d_S^b = {}^{1/2}k$ is the Stokes depth scale. For random directional waves, the Stokes drift velocity is (Kenyon, 1969)

Table A1
The e-Folding Depths of the Stokes Drift and the Wave Dissipation Under the 10-m Wind Speed Conditions of 5, 10, 15, and 20 m/s

U_{10} (m/s)	5	10	15	20
d_S (m)	0.8332	3.1111	7.3992	14.2268
d_{ds} (m)	0.4748	1.4887	3.4095	6.2139

$$\mathbf{U}_S(z) = (U_{Sx}, U_{Sy}) = 2\int \mathbf{k}e^{2kz}E(k,\theta)dkd\ \theta, \tag{A.2}$$

where $E(k,\theta)$ is the wave spectrum.

The bulk formulation of the Stokes drift deduced from equation (A.1) is widely used in the estimation of the wave-affected wind energy input in the Ekman layer (Liu et al., 2007; Wu & Liu, 2008; Zhang et al., 2013). However, according to Tamura et al. (2012), the bulk formulation significantly underestimated the surface Stokes drift and overestimated the Stokes depth. To obtain a precise expression of the Stokes drift for a realistic ocean wavefield, Tamura et al. (2012) parameterized equation (A.2) as

$$\mathbf{U}_S^p(z) = \mathbf{U}_{S0} \exp\left(\frac{z}{d_S}\right), \tag{A.3}$$

with the Stokes drift velocity at the sea surface $\mathbf{U}_{S0}$ and the Stokes *e*-folding depth d_S.

The wave dissipation process is also parameterized according to this approach. The wave dissipation is (Jenkins, 1989)

$$\mathbf{T}^{ds} = 2\int \omega \mathbf{k}e^{2kz}S_{ds}(k,\theta)dkd\ \theta, \tag{A.4}$$

where $S_{ds}(k,\theta)$ is the wave dissipation source term. Similar to the parameterization of the Stokes drift in equation (A.3), we parameterize the wave dissipation as

$$\mathbf{T}^{ds,p}(z) = \mathbf{T}_0^{ds} \exp\left(\frac{z}{d_{ds}}\right) \tag{A.5}$$

with the wave dissipation at the sea surface $\mathbf{T}_0^{ds}$ and its *e*-folding depth d_{ds}.
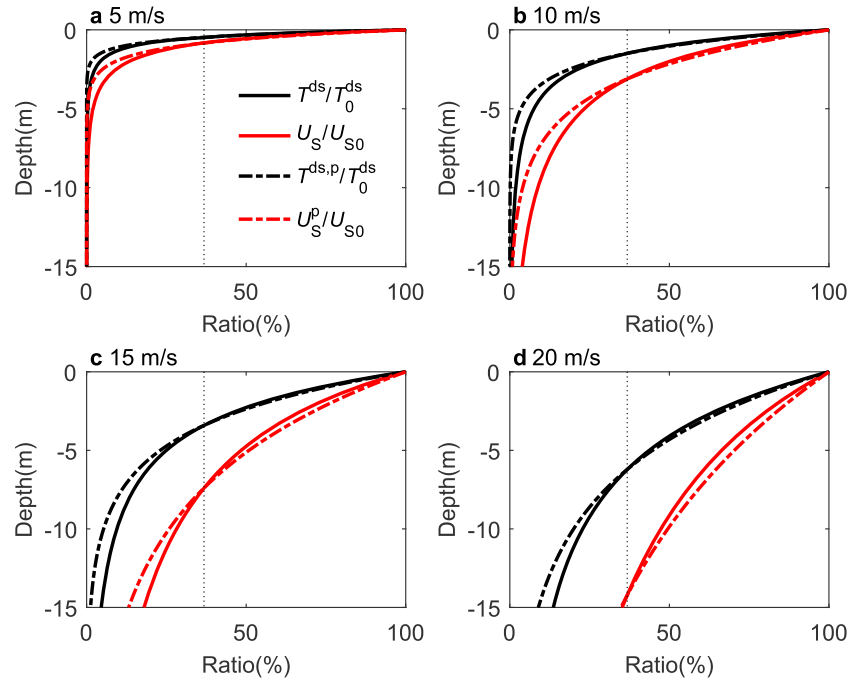
Figure A1. Ratios of the Stokes drift and the wave dissipation in relative to their surface strength under various 10-m wind speeds: (a) 5 m/s, (b) 10 m/s, (c) 15 m/s, and (d) 20 m/s. The black dashed line represents the *e*-folding scale. U_{S0} and T_0^{ds} represent the Stokes drift and the wave dissipation at the surface. U_S^p and $T^{ds,p}$ are the parameterized Stokes drift and wave dissipation. U_S and T^{ds} are the original definitions of Stokes drift and wave dissipation based on the wave spectrum.

We validated the aforementioned parameterizations with the wave spectrum for the fully developed sea by Donelan and Pierson (1987) according to equations (44)–(47). Given that $E(k, \theta) = E(k, -\theta)$,

$$U_{Sy} = T_y^{ds} = 0, \tag{A.6}$$

$$U_S(z) = U_{Sx}(z) = 4\sqrt{g}\int_0^\infty \int_0^\pi k^{3/2} \exp(2kz) \cos(\theta) E(k, \theta) d\,\theta dk, \tag{A.7}$$

$$T^{ds}(z) = T_x^{ds}(z) = 4\sqrt{g}\int_0^\infty \int_0^\pi k^{3/2} \exp(2kz) \cos(\theta) S_{ds}(k, \theta) d\,\theta dk. \tag{A.8}$$

The estimated Stokes e-folding depths and the e-folding depth of wave dissipation are given in Table A1. Figure A1 illustrates the comparison of the parameterized Stokes drift and wave dissipation in equations (A.3) and (A.5) with their original definitions in equations (A.2) and (A.4) at various 10-m wind speeds. For the water column above the e-folding depth, the parameterized Stokes drift and the wave dissipation are in good agreement with their original definitions, especially at low wind speed (Figures A1a and A1b). Such parameterizations lightly overestimate the Stokes drift and wave dissipation only under extremely high wind speed conditions (Figures A1c and A1d). Therefore, we combined this parameterization scheme with equations (13) and (14) to estimate the wind stress energy input and wave-induced energy input.

References

Alford, M. H. (2003). Improved global maps and 54-year history of wind-work on ocean inertial motion. *Geophysical Research Letters*, *30*(8), 1424. https://doi.org/10.1029/2002GL016614

Ardhuin, F., Marie, L., Rascle, N., Forget, P., & Roland, A. (2009). Observation and estimation of Lagrangian, Stokes, and Eulerian currents induced by wind and waves at the sea surface. *Journal of Physical Oceanography*, *39*(11), 2820–2838. https://doi.org/10.1175/2009JPO4169.1

Ardhuin, F., Rascle, N., & Belibassakis, K. A. (2008). Explicit wave-averaged primitive equations using a generalized Lagrangian mean. *Ocean Modelling*, *20*, 35–60. https://doi.org/10.1016/j.ocemod.2007.07.001

Atlas, R., Hoffman, R. N., Ardizzone, J., Leidner, S. M., & Jusem, J. C. (2009). Development of a new cross-calibrated, multi-platform (CCMP) ocean surface wind product. Paper presented at AMS 13th Conference on Integrated Observing and Assimilation System for Atmosphere, Oceans, and Land Surface, Phoenix, AZ.

Donelan, M. A., Curcic, M., Chen, S. S., & Magnusson, A. K. (2012). Modeling waves and wind stress. *Journal of Geophysical Research*, *117*, C00J23. https://doi.org/10.1029/2011JC007787

Donelan, M. A., & Pierson, W. J. P. (1987). Radar scattering and equilibrium ranges in wind-generated waves with application to scatterometry. *Journal of Geophysical Research*, *92*, 4971–5029. https://doi.org/10.1029/JC092iC05p04971

Ekman, V. W. (1905). On the influence of the Earth's rotation on ocean currents. *Arkiv for Matematik, Astronomioch Fysik*, *2*, 1–52.

Elipot, S., & Gille, S. (2009). Ekman layers in the Southern Ocean: Spectral models and observations, vertical viscosity and boundary layer depth. *Ocean Science*, *5*, 115–139. https://doi.org/10.5194/osd-6-277-2009

Hasselmann, S., Hasselmann, K., Allender, J. H., & Barnett, T. P. (1985). Computation and parameterizations of the nonlinear energy transfer in a gravity-wave spectrum. Part II: Parameterizations of the nonlinear energy transfer for application in wave models. *Journal of Physical Oceanography*, *15*(11), 1378–1391. https://doi.org/10.1175/1520-0485(1985)015<1378:CAPOTN>2.0.CO;2

Hasselmann, S., Hasselmann, K., Komen, G. K., Zhang, Y., Song, Z., Wu, K., & Shi, Y. (1988). The WAM model—A third generation ocean wave prediction model. *Journal of Physical Oceanography*, *18*(12), 1775–1810. https://doi.org/10.1175/1520-0485(1988)018<1775:TWMTGO>2.0.CO;2

Huang, R. X., Wang, W., & Liu, L. L. (2006). Decadal variability of wind energy input to the world ocean. *Deep Sea Research Part II*, *53*(1-2), 31–41. https://doi.org/10.1016/j.dsr2.2005.11.001

Hui, Z., & Xu, Y. (2016). The impact of wave-induced Coriolis-Stokes forcing on satellite-derived ocean surface currents. *Journal of Geophysical Research: Oceans*, *121*, 410–426. https://doi.org/10.1002/2015JC011082

Jenkins, A. D. (1987). Wind and wave induced currents in a rotating sea with depth-varying eddy viscosity. *Journal of Physical Oceanography*, *17*, 938–951. https://doi.org/10.1175/1520-0485(1987)017<0938:WAWICI>2.0.CO;2

Jenkins, A. D. (1989). The use of a wave prediction model for driving a near surface current model. *Deutsche Hydrographische Zeitschrift*, *42*, 134–149. https://doi.org/10.1007/BF02226291

Kantha, L. H., Wittmann, P., Sclavo, M., & Carniel, S. (2009). A preliminary estimate of the Stokes dissipation of wave energy in the global ocean. *Geophysical Research Letters*, *36*, L02605. https://doi.org/10.1029/2008GL036193

Kenyon, K. E. (1969). Stokes drift for random gravity waves. *Journal of Geophysical Research*, *74*, 6991–6994. https://doi.org/10.1029/JC074i028p06991

Komen, G. J., Cavaleri, L., Donelan, M., Hasselmann, K., Hasselmann, S., & Janssen, P. A. E. M. (1995). *Dynamics and modelling of ocean waves* (pp. 339). Cambridge University Press. ISBN0521470471.

Lewis, D. M., & Belcher, S. E. (2004). Time-dependent, coupled, Ekman boundary layer solutions incorporating Stokes drift. *Dynamics of Atmospheres and Oceans*, *37*, 313–351. https://doi.org/10.1016/j.dynatmoce.2003.11.001

Lin, X., Zhai, X., Wang, Z., & Munday, D. R. (2018). Mean, variability, and trend of Southern Ocean wind stress: Role of wind fluctuations. *Journal of Climate*, *31*, 3557–3573. https://doi.org/10.1175/JCLI-D-17-0481.1

Liu, B., Wu, K. J., & Guan, C. L. (2007). Global estimates of wind energy input to subinertial motions in the Ekman-Stokes layer. *Journal of Oceanography*, *63*, 457–466. https://doi.org/10.1007/s10872-007-0041-6

Liu, B., Wu, K. J., & Guan, C. L. (2009). Wind energy input to the Ekman-Stokes layer: Reply to comment by Jeff A Polton. *Journal of Oceanography*, *65*(5), 669–673. https://doi.org/10.1007/s10872-009-0058-0

Lund, B., Zappa, C. J., Graber, H. C., & Cifuentes-Lorenzen, A. (2017). Shipboard wave measurements in the Southern Ocean. *Journal of Atmospheric and Oceanic Technology*, *34*, 2113–2126. https://doi.org/10.1175/JTECH-D-16-0212.1

Perrie, W., Tang, C. L., Hu, Y., & DeTracy, B. M. (2003). The impact of waves on surface currents. *Journal of Physical Oceanography*, *33*(10), 2,126–2,140. https://doi.org/10.1175/1520-0485(2003)033<2126:TIOWOS>2.0.CO;2

Phillips, O. M. (1977). *The Dynamics of the Upper Ocean* (2nd ed.). Cambridge-London-New York-Melbourne: Cambridge University Press.

Polton, J. A. (2009). A wave-averaged energy equation: comment on "global estimates of wind energy input to subinertial motions in the Ekman-Stokes layer" by Bin Liu, Kejian Wu and Changlong Guan. *Journal of Oceanography*, *65*(5), 665–668. https://doi.org/10.1175/2008JPO3943.1

Polton, J. A., Lewis, D. M., & Belcher, S. E. (2005). The role of wave-induced Coriolis-Stokes forcing on the wind-driven mixed layer. *Journal of Physical Oceanography*, *35*, 444–457. https://doi.org/10.1175/JPO2701.1

Price, J., & Sundermeyer, M. A. (1999). Stratified Ekman layers. *Journal of Geophysical Research*, *104*, 20,467–20,494. https://doi.org/10.1029/1999JC900164

Rascle, N., Ardhuin, F., & Queffeulou, P. (2008). A global wave parameter database for geophysical applications. Part I, Wave-current–turbulence interaction parameters for the open ocean based on traditional parameterizations. *Ocean Modelling*, *25*, 154–171. https://doi.org/10.1016/j.ocemod.2008.07.006

Rascle, N., Ardhuin, F., & Terray, E. A. (2006). Drift and mixing under the ocean surface: A coherent one-dimensional description with application to unstratified conditions. *Journal of Geophysical Research*, *111*, C03016. https://doi.org.10.1029/2005JC003004

Rimac, A., von Storch, J.-S., & Eden, C. (2016). The total energy flux leaving the ocean's mixed layer. *Journal of Physical Oceanography*, *46*(6), 1,885–1,900. https://doi.org/10.1175/JPO-D-15-0115.1

Rimac, A., von Storch, J.-S., Eden, C., & Haak, H. (2013). The influence of high-resolution wind stress field on the power input to near-inertial motions in the ocean. *Geophysical Research Letters*, *40*, 4882–4886. https://doi.org/10.1002/grl.50929

Santiago-Mandujano, F., & Firing, E. (1990). Mixed-layer shear generated by wind stress in the central equatorial Pacific. *Journal of Physical Oceanography*, *20*, 1576–1582. https://doi.org/10.1175/1520-0485(1990)020<1576:MLSGBW>2.0.CO;2

Sayol, J. M., Orfila, A., & Oey, L. Y. (2016). Wind induced energy–momentum distribution along the Ekman–Stokes layer. Application to the Western Mediterranean Sea climate. *Deep-Sea Research Part I*, *111*, 34–49. https://doi.org/10.1016/j.dsr.2016.01.004

Song, J. B. (2009). The effects of random surface waves on the steady Ekman current solutions. *Deep-Sea Research Part I*, *56*, 659–671. https://doi.org/10.1016/j.dsr.2008.12.014

Swart, N. C., & Fyfe, J. C. (2012). Observed and simulated changes in the Southern Hemisphere surface westerly wind-stress. *Geophysical Research Letters*, *39*, L16711. https://doi.org/10.1029/2012GL052810

Swart, N. C., Fyfe, J. C., Gillett, N., & Marshall, G. J. (2015). Comparing trends in the Southern Annular Mode and surface westerly jet. *Journal of Climate*, *28*, 8840–8859. https://doi.org/10.1175/JCLI-D-15-0334.1

Tamura, H., Miyazawa, Y., & Oey, L. Y. (2012). The Stokes drift and wave induced-mass flux in the North Pacific. *Journal of Geophysical Research*, *117*, C08021. https://doi.org/10.1029/2012JC008113

Tang, C. L., Perrie, W., Jenkins, A. D., DeTracey, B. M., Hu, Y., Toulany, B., & Smith, P. C. (2007). Observation and modeling of surface currents on the Grand Banks: A study of the wave effects on surface currents. *Journal of Geophysical Research*, *112*, C10025. https://doi.org/10.1029/2006JC004028

Tolman, H. L., & Chalikov, D. (1996). Source terms in a third-generation wind-wave model. *Journal of Physical Oceanography*, *26*, 2497–2518. https://doi.org/10.1175/1520-0485(1996)026<2497:STIATG>2.0.CO;2

Wang, W., & Huang, R. X. (2004). Wind energy input to the Ekman layer. *Journal of Physical Oceanography*, *34*, 1,267–1,275. https://doi.org/10.1175/1520-0485(2004)034<1267:WEITTE>2.0.CO;2

Watanabe, M., & Hibiya, T. (2002). Global estimates of the wind-induced energy flux to inertial motions in the surface mixed layer. *Geophysical Research Letters*, *29*(8), 1239. https://doi.org/10.1029/2001GL014422

Webb, A., & Fox-Kemper, B. (2011). Wave spectral moments and Stokes drift estimation. *Ocean Modelling*, *40*, 273–288. https://doi.org/10.1016/j.ocemod.2011.08.007

Wu, J. (1982). Wind-stress coefficients ver sea surface from breeze to hurricane. *Journal of Geophysical Research*, *87*(C12), 9,704–9,706. https://doi.org/10.1029/JC087iC12p09704

Wu, K. J., & Liu, B. (2008). Stokes drift-induced and direct wind energy inputs into the Ekman layer within the Antarctic Circumpolar Current. *Journal of Geophysical Research*, *113*, C10002. https://doi.org/10.1029/2007JC004579

Wunsch, C. (1998). The work done by the wind on the oceanic general circulation. *Journal of Physical Oceanography*, *28*, 2,332–2,340. https://doi.org/10.1175/1520-0485(1998)028<2332:TWDBTW>2.0.CO;2

Yang, X. Y., Huang, R. X., & Wang, J. (2008). Delayed baroclinic response of the Antarctic circumpolar current to surface wind stress. *Science in China: Series D*, *51*(7), 1036–1043. https://doi.org/10.1007/s11430-008-0074-8

Young, I. R. (1999). Seasonal variability of the global ocean wind and wave climate. *International Journal of Climatology*, *19*, 931–950. https://doi.org/10.1002/(SICI)1097-0088(199907)19:9<931:AID-JOC412>3.0.CO;2-O

Zhang, Y. M., Wu, K. J., Zhang, X. S., Bi, F., Song, Z. Y., & Liu, S. H. (2013). Improving the estimate of wind energy input into the Ekman layer within the Antarctic Circumpolar Current. *Acta Oceanologica Sinica*, *32*(3), 19–27. https://doi.org/10.1007/s13131-013-0284-6